



Hole traps in $\text{Lu}_2\text{O}_3:\text{Eu}$ ceramic scintillators. II. Radioluminescence and thermoluminescence

R.H. Bartram^{a,*}, A. Lempicki^b, L.A. Kappers^a, D.S. Hamilton^a

^aPhysics Department, University of Connecticut, Storrs, CT 06269-3046, USA

^bALEM Association, 303A Commonwealth Avenue, Boston MA 02115, USA

Received 12 December 2002; received in revised form 14 August 2003; accepted 24 September 2003

Abstract

A sample of Eu^{3+} -activated lutetium sesquioxide transparent ceramic has been investigated by combined scintillation and thermoluminescence excited by prolonged gamma-ray irradiation. The thermoluminescence glow curve partially confirms and extends a previous model for afterglow following pulsed X-ray excitation. The initial concentration of hole traps, tentatively attributed to anion Frenkel defects in thermodynamic equilibrium, is found to be substantially augmented by reversible radiation damage.

© 2003 Elsevier B.V. All rights reserved.

Keywords: Ceramic scintillators; Radioluminescence; Thermoluminescence; $\text{Lu}_2\text{O}_3:\text{Eu}$

1. Introduction

The observed persistence of the afterglow of ceramic $\text{Lu}_2\text{O}_3:\text{Eu}$ following pulsed X-ray excitation was attributed to thermal ionization from multiple hole traps with a range of trap depths, and a computational model with a quasi-continuous effective distribution of trap depths was presented that fits the persistent afterglow out to 5 min following the exciting pulse [1]. The present paper is concerned with a complementary investigation of hole traps in another sample of the same material by a technique combining radioluminescence and thermoluminescence, designed to test and augment the model over an extended range of trap depths.

2. Experimental methods

It is difficult to assess the extent to which the competing process of carrier trapping diminishes the efficiency of scintillator response from thermoluminescence data alone in the absence of absolute light output measurements. Accordingly, an experiment was initiated with the objective of determining the branching ratio of electron–hole pairs that contribute either to thermoluminescence or to scintillation [2,3]. Energy storage by deep traps is probed by comparison of thermoluminescence and scintillation light outputs, facilitated by a common apparatus and detection scheme for both measurements. This scheme exploits a common activator with identical emission spectra for both thermoluminescence and scintillation. A schematic diagram of the experimental arrangement is shown in Fig. 1. An electron Van de Graaff

*Corresponding author.

E-mail address: rhbartram2@aol.com (R.H. Bartram).

accelerator, operated at 1.0 MV and 1.0 μA , is employed as the primary radiation source with the electron beam stopped by a thin copper target that

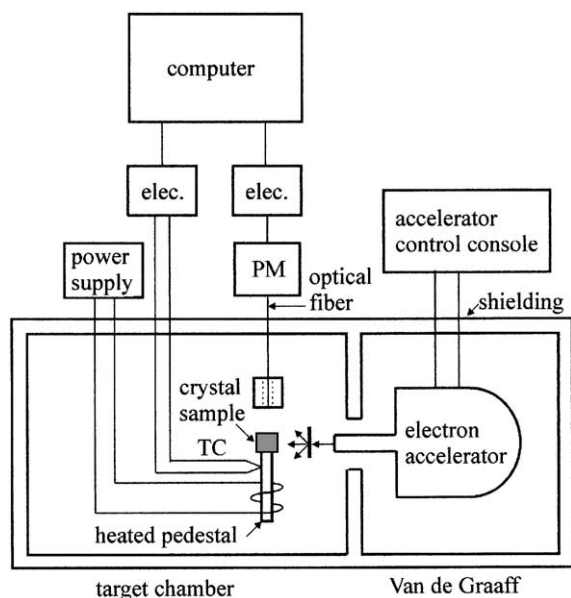


Fig. 1. Schematic diagram of experimental setup.

serves as an approximate point source of gamma rays. The sample is mounted on a copper pedestal enclosing a heating element. Sample temperature is monitored by means of a thermocouple attached to the pedestal, and luminescence is extracted by a shielded optical fiber and detected by a photomultiplier. Both the photomultiplier and thermocouple outputs are passed via electrometers to a personal computer, with data recorded at 4 s intervals for radiation times ranging from 15 s to 16 min. An unusually rapid temperature-ramp rate was adopted to facilitate the comparison of thermoluminescence and scintillation light outputs on comparable scales and to expedite data acquisition. The sample of ceramic $\text{Lu}_2\text{O}_3:\text{Eu}$ employed in the present investigation was cut in the form of a rectangular parallelepiped with dimensions 2 mm \times 3 mm \times 8 mm. The activator concentration was 5 mol%.

3. Experimental results

Recorded light output and sample temperature as functions of time are plotted for an irradiation

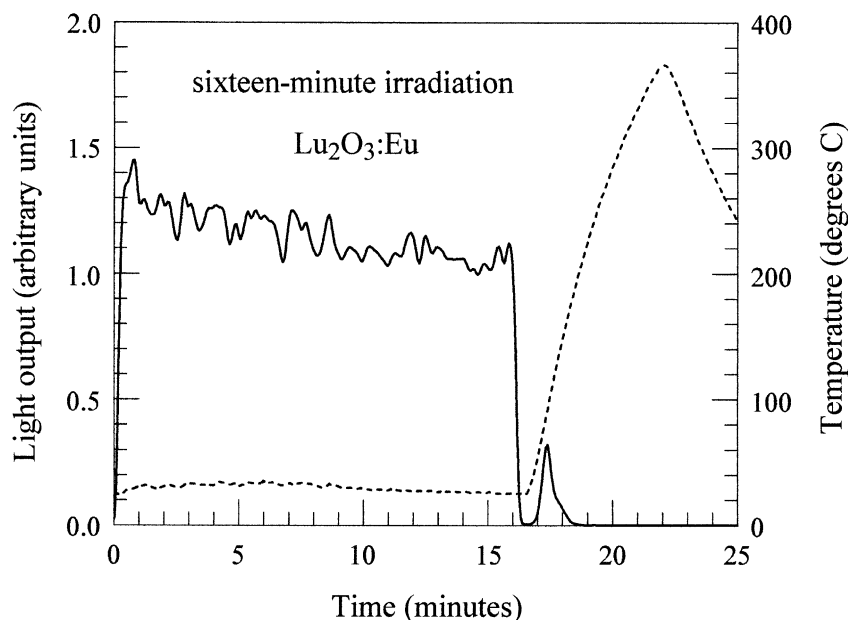


Fig. 2. Recorded light output (continuous curve) and sample temperature (dashed curve) as functions of time for 16 min irradiation of Eu : Lu_2O_3 ceramic scintillator.

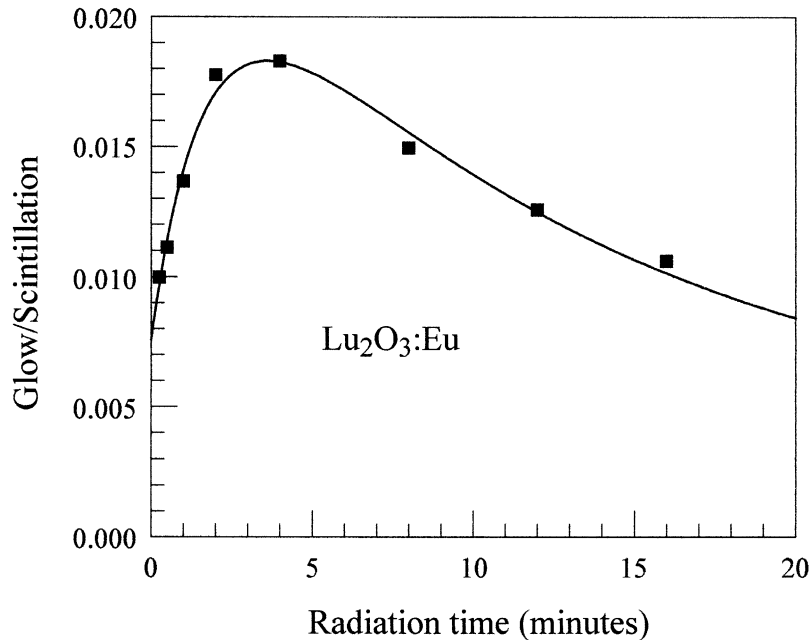


Fig. 3. Ratio of integrated thermoluminescence light output G to integrated scintillation light output S as a function of radiation time for Eu : Lu_2O_3 ceramic scintillator. Recorded experimental data are represented by filled squares, and the continuous curve is a plot of Eq. (12) with optimized parameters.

time of 16 min in Fig. 2. The ratio of integrated thermoluminescence light output to the integrated scintillation light output (glow/scintillation or G/S) is plotted as a function of radiation time in Fig. 3.

4. Analysis of glow curve

Two overlapping Gaussian distributions of trap depths were assumed in the computational model of persistent afterglow [1], and their continuous distribution was simulated by 22 discrete traps with trap depths ranging from 0.58 to 1.0 eV at intervals of 0.02 eV. The relative trapping parameters were given by

$$G_i = \frac{g_i}{\sum_{i=1}^R g_i}, \quad (1a)$$

Table 1
Optimized parameters for logarithmic least-squares fit to experimental data

Parameter	Value
E_1 (eV)	0.4422
σ_1 (eV)	0.0877
E_2 (eV)	0.9849
σ_2 (eV)	0.1073
B	3.128

$$g_i = B \exp \left[-\frac{(E_{\text{TRAP}i} - E_1)^2}{2\sigma_1^2} \right] + \exp \left[-\frac{(E_{\text{TRAP}i} - E_2)^2}{2\sigma_2^2} \right]. \quad (1b)$$

The corresponding optimized parameters are listed in Table 1.

A simulated glow curve was constructed from the second term in Eq. (1b) only, since the traps

described by the first term are too shallow to make an appreciable contribution to the thermoluminescence. A linear temperature ramp was assumed with slope $R = 90 \text{ K min}^{-1}$ corresponding to the early portion of the heating phase. First-order kinetics was assumed since the cross-section for re-trapping is much smaller than that for recombination in this material. The concentrations of trapped holes are then given by

$$n_i(t)/n_0 = G_i \exp \left\{ -s \left(\frac{E_{\text{TRAP}i}}{k_B R} \right) \times \left[\frac{\exp(-E_{\text{TRAP}i}/k_B T(t))}{E_{\text{TRAP}i}/k_B T(t)} - \text{Ei} \left(\frac{E_{\text{TRAP}i}}{k_B T(t)} \right) - \frac{\exp(-E_{\text{TRAP}i}/k_B T(0))}{E_{\text{TRAP}i}/k_B T(0)} + \text{Ei} \left(\frac{E_{\text{TRAP}i}}{k_B T(0)} \right) \right] \right\}, \quad (2a)$$

$$\text{Ei}(x) = \int_x^\infty \frac{\exp(-y)}{y} dy, \quad (2b)$$

$$n_0 = \sum_i n_i(0), \quad (2c)$$

$$k_B = 8.6174 \times 10^{-5} \text{ eV/K}, \quad (2d)$$

where k_B is Boltzmann's constant and $\text{Ei}(x)$ is the exponential integral. The frequency factor was assumed to have the value $s = 10^{12} \text{ s}^{-1}$ as in the afterglow simulation. The light output is then given by

$$LO(t) \propto \sum_i p_i(t) n_i(t) / n_0, \quad (3a)$$

$$p_i(t) = s \exp[-E_{\text{TRAP}i}/k_B T(t)]. \quad (3b)$$

A simulated glow curve was calculated from these equations for 101 equally spaced trap depths ranging from 0.95 to 1.5 eV at intervals of 0.0055 eV. The experimental glow curve of Fig. 2 for a 16 min irradiation is plotted on an expanded scale in Fig. 4, together with the simulated glow curve. Only the minimum trap depth (0.95 eV) was adjusted in the simulation to match the initial rise of the experimental glow curve; traps of this depth retain 90% of their charge for 16 min, the

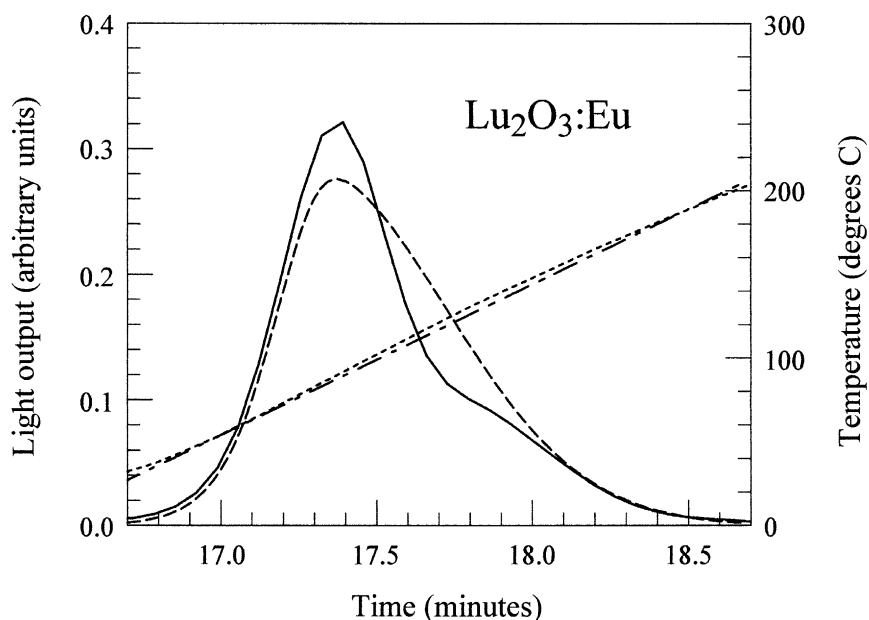


Fig. 4. Thermoluminescence glow curve of Fig. 2, displayed on an expanded scale, (solid line) compared with the simulated glow curve based on the trap-depth distribution derived from afterglow (dashed line). Also plotted are the recorded temperature (dotted line) and the linear temperature ramp assumed in the simulation (dot-dash line).

duration of the scintillation phase, and are thus expected to contribute significantly to thermoluminescence. The traps more shallow than that were assumed to be substantially thermally ionized during the scintillation phase and thus would not contribute significantly to thermoluminescence. The remaining parameter values were those specified in Table 1.

5. Rate equations

The initial rise in G/S as a function of irradiation time in Fig. 3 is a new feature, not previously encountered in this type of experiment, that can be explained in terms of reversible radiation damage. For the present purpose, the rate equations can be simplified by lumping together all the hole traps that are deep enough to contribute to thermoluminescence in a single concentration n , and by ignoring the more shallow traps whose effects are undetectable in this experiment. On the other hand, we introduce the complication that the trap concentration is increased by irradiation to a saturation level. The resulting equations for the scintillation phase are:

$$\frac{dn_v}{dt} = f - n_v n_e A_r - n_v(N - n)A, \quad (4a)$$

$$\frac{dN}{dt} = N_m r(1 - N/N_m), \quad (4b)$$

$$\frac{dn}{dt} = n_v(N - n)A, \quad (4c)$$

$$\frac{dn_e}{dt} = f - n_v n_e A_r, \quad (4d)$$

$$\frac{dn_a}{dt} = n_v n_e A_r - n_a \tau_r^{-1}, \quad (4e)$$

where n_v is the concentration of valence-band holes, n_e is the concentration of electrons captured by activators (Eu^{2+}), n is the concentration of trapped holes, N is the concentration of deep hole traps with initial value N_0 and maximum value N_m , and n_a is the concentration of excited activators (Eu^{3+*}). Parameters include the rate of electron–hole pair production f , the radiative recombination rate A_r , the trapping rate A , the

trap generation rate parameter r and the radiative lifetime τ_r . Valence-band holes are assumed to be trapped instantaneously at the activators. The different excited states of the activator are not distinguished since relaxation to the lowest $^5\text{D}_0$ state by a cascade process occurs too rapidly ($<100 \mu\text{s}$) to be detectable in the present experiment.

We can eliminate Eq. (4d) by the relation

$$\frac{dn_e}{dt} = \frac{dn_v}{dt} + \frac{dn}{dt} \rightarrow n_e = n_v + n + n_{e0}, \quad (5)$$

where n_{e0} is the initial concentration of electrons trapped on activators (Eu^{2+}).

Solution of the rate equations is facilitated by the additional approximations

$$\frac{dn_v}{dt} \cong 0, \quad (6a)$$

$$\frac{dn_a}{dt} \cong 0. \quad (6b)$$

Transients in these concentrations are not detectable on the time scale of the experiment, and they are otherwise slowly varying. Eq. (4e) is then replaced by the following approximate expression for the light output:

$$LO \equiv n_a \tau_r^{-1} \cong n_v n_e A_r. \quad (7)$$

In addition, the concentration of valence-band holes is given approximately by

$$n_v \cong \frac{f}{n_e A_r + (N - n)A} \cong \frac{f}{n_e A_r} \cong \frac{f}{n_{e0} A_r}, \quad (8)$$

where the second approximation reflects the observation that the rate of hole trapping is less than 2% of the rate of radiative recombination, and the third approximation reflects the inequality

$$n_{e0} \gg n, n_v \quad (9)$$

required for consistency with the data, as will become apparent. Thus n_v is approximately independent of irradiation time.

The remaining equations (4b) and (4c) have the respective solutions

$$N = N_0 + (N_m - N_0)[1 - \exp(-rt)], \quad (10)$$

$$n = N_m \left\{ 1 - \exp(-ct) - \left(\frac{1 - N_0/n_m}{1 - r/c} \right) \times [\exp(-rt) - \exp(-ct)] \right\}, \quad (11a)$$

$$c \equiv n_v A \quad (11b)$$

and the ratio of integrated thermoluminescence light output to integrated scintillation light output (G/S) is given by

$$G/S = n/(ft - n) \cong n/ft. \quad (12)$$

Eqs. (11) depend on the inequality in Eq. (9).

6. Computational results

Eqs. (11) and (12) were fit to experimental data with the result shown in Fig. 3. Optimized parameters are listed in Table 2.

Some relevant material properties of Lu₂O₃ : Eu ceramic are listed in Table 3 including density ρ , lutetium concentration N_{Lu} , activator concentration N_a at 5 mol% doping, radiative lifetime τ_r of the Eu³⁺ ⁵D₀ excited state, estimated bandgap energy E_g and the number n_{eh} of electron–hole

Table 2
Optimized parameters for fit to G/S

Parameter	Value
r (min ⁻¹)	0.181
c (min ⁻¹)	0.829
N_m/N_0	19.0
N_0/f (min)	0.00915

Table 3
Material properties of Lu₂O₃ : Eu ceramic

Parameter	Value
ρ (g cm ⁻³)	9.4
N_{Lu} (cm ⁻³)	2.8×10^{22}
N_a (cm ⁻³) (5%)	1.4×10^{21}
τ_r^{-1} (min ⁻¹)	6×10^4
E_g (eV)	5.4
n_{eh} (MeV ⁻¹)	82.504

Table 4
Derived parameters

Parameter	Value
f (cm ⁻³ min ⁻¹)	6×10^{16}
N_0 (cm ⁻³)	6×10^{14}
N_m (cm ⁻³)	10^{16}
n_a (cm ⁻³)	10^{12}
$N_0 A/n_{e0} A_r$	0.00759
$n_{e0} A_r$ (min ⁻¹)	$\geq 3 \times 10^9$
n_v (cm ⁻³)	$\leq 2 \times 10^7$
A (cm ³ min ⁻¹)	$\geq 4 \times 10^{-8}$
n_{e0} (cm ⁻³)	$\geq 10^{16}$

pairs per MeV calculated by the method of Bartram and Lempicki [4].

The gamma-ray energy deposited in the sample during the present experiment is presumably comparable with that for LuAP, 2.0 mW cm⁻³ [2]. The value of f listed in Table 4 estimated from the rate of energy deposition and the value of n_{eh} from Table 3, provides a basis for evaluating N_0 and N_m as well, also listed in Table 4. Together with τ_r^{-1} and Eqs. (7) and (8), f also provides the basis for evaluating the concentration n_a of excited activators.

The ratio $N_0 A/n_{e0} A_r$ listed in Table 4 is provided by the initial value of G/S . Other entries in Table 4 include an inequality satisfied by $n_{e0} A_r$ derived from the observation that the rise time of the ⁵D₃ excited state appears to be less than 20 ns [1]. A corresponding inequality satisfied by n_v follows from Eq. (8). A bound on A is derived from the preceding entries. The inequality for n_{e0} is provided by Eq. (9) and the fact that n approaches N_m after prolonged irradiation.

7. Conclusions

One can infer from the average value of G/S in Fig. 3 that only 1.2% of holes are trapped, while 98.8% recombine radiatively; thus deep traps have little adverse effect on the transfer efficiency of this material. Although G/S is not constant, it is also evident that the deep traps approach saturation only near the maximum dose in this experiment.

The model for extended afterglow [1] is amply confirmed by the resemblance of the recorded glow curve and the simulated glow curve in Fig. 4. However, the recorded glow curve reveals additional structure in the trap-depth distribution that is obscured during afterglow by repeated redistribution of holes among traps.

It is evident from the present analysis that pre-existing trapped electrons play a dominant role and consequently, that the rate equations are effectively linear apart from the radiation damage and saturation effects. The quality of fit of the solid curve in Fig. 3, based on Eqs. (9)–(12) with optimized parameters listed in Table 2, confirms the assumption of a large initial concentration of Eu^{2+} . If there were no pre-existing trapped electrons then the curve of G/S in Fig. 3 would be proportional to $1/t$ near the origin, since the initial rate of trapping would be linear, and the initial scintillation light output quadratic, functions of the radiation dose. Nevertheless, the fraction of europium activators that are initially in the $2+$ charge state, $\gg 0.001\%$, may still be very small. A plausible speculation is that Eu^{2+} may be charge-compensated by oxygen vacancies.

The trap-depth distributions described by Eq. (1) with the parameters of Table 1 suggest that there are two distinct types of traps involved, both of which are perturbed by strains and by proximity to grain boundaries in the ceramic scintillator material. A plausible model for a deep hole trap is an anion occupying an interstitial site. A relevant feature of the cubic bixbyite structure of lutetium sesquioxide, space group $T_h^7(\text{Ia}3)$, is its derivation from the fluorite structure [5], as noted in the accompanying paper [1]. The arrangement of anions in the two structures is similar except that one-quarter of the anion sites in the fluorite structure are replaced by empty interstitial sites in the bixbyite structure that could readily accommodate a displaced anion, thus favoring the formation of anion Frenkel defects (oxygen vacancy–interstitial pairs). The initial trap concentration N_0 may then correspond to the anion Frenkel defect concentration in thermodynamic equilibrium at constant temperature and pressure [6],

$$N_0 = \sqrt{N_{\text{Oxygen}} N_{\text{interstitial}}} \exp(-g/2k_{\text{B}}T), \quad (13)$$

where g is the formation Gibbs free energy. The temperature T in Eq. (13) is the lowest temperature at which vacancies are mobile on the time scale of the annealing process; that defect concentration is frozen in at lower temperatures. Additional defects may be generated by irradiation, thus creating additional hole traps. The maximum trap concentration N_m is then determined by the dynamic equilibrium between radiation-induced defect generation and radiation-enhanced recombination of vacancies with interstitials. The initial trap concentration N_0 is reset each time the sample is heated to 400°C to monitor thermoluminescence and is subsequently annealed.

Experiments are in progress to investigate shallow traps contributing to persistent afterglow by combining radioluminescence and thermoluminescence at low temperature. Preliminary results suggest that the shallow traps may have a different origin than the deep traps, since they exhibit neither radiation-damage nor saturation effects. Surface states at grain boundaries are possible candidates for shallow traps since they are expected to be abundant in this ceramic material.

The trap concentration N was specified in the afterglow simulation [1] as comprising those hole traps with depths between 0.58 and 1.0 eV, and in the glow-curve simulation as comprising those hole traps deeper than 0.95 eV. (Obviously, there is some overlap in these specifications.) The ratio of these concentrations calculated from Eq. (1b) with the parameters of Table 1 is $N_{\text{thermo}}/N_{\text{after}} = 0.890$, and the value of α inferred from afterglow simulation [1] is $\alpha = 0.0231 \equiv \alpha_{\text{after}}$; accordingly, the predicted value of α_{thermo} , defined by

$$\begin{aligned} \alpha_{\text{thermo}} &\equiv N_{\text{thermo}}A/n_{\text{e}0}A_{\text{r}} \\ &= (N_{\text{thermo}}/N_{\text{after}})\alpha_{\text{after}}, \end{aligned} \quad (14)$$

is $\alpha_{\text{thermo}} = 0.0206$. The actual values inferred from Table 4 are an initial value $\alpha_0 = 0.00759$ and a final value $\alpha_m = 0.144$ after radiation damage, bracketing the predicted value. The difference between the predicted and the initial values may be attributable to limited radiation damage under pulsed X-ray excitation.

Acknowledgements

We gratefully acknowledge the partial support of this work by the National Institutes of Health, Public Health Service, Department of Health and Human Services, under Grants No. 2R44-DE12785-02A1 and N44-NS-0-2306.

References

- [1] C. Brecher, R.H. Bartram, A. Lempicki, *J. Lumin.* 106 (2004) 159, preceding article in this issue.
- [2] R.H. Bartram, D.S. Hamilton, L.A. Kappers, A. Lempicki, *J. Lumin.* 75 (1997) 183.
- [3] R.H. Bartram, D.S. Hamilton, L.A. Kappers, A. Lempicki, J. Glodo, J.S. Schweitzer, C.L. Melcher, *Radiat. Eff. Defects Solids* 150 (1999) 11.
- [4] R.H. Bartram, A. Lempicki, *J. Lumin.* 68 (1996) 225.
- [5] R.W.G. Wyckoff, *Crystal Structures*, 2nd Edition, Vol. 2, Interscience, New York, 1963–1971, pp. 2–6.
- [6] A.B. Lidiard, A.R. Allnatt, *Atomic Transport in Solids*, Cambridge University Press, Cambridge, 1994.